CCAT-p science case for GEco

Peter Schilke, Doug Johnstone, Rene Plume, Erik Rosolowsky, Robert Simon, Friedrich Wyrowski

1   Introduction

The star formation rate is governed by the flow of gas from galactic scales down to individual star-forming cores. Thus the star formation rate depends on a variety of physical processes that take place on physical scales between those within individual molecular clouds and those of galactic disks (i.e. from Mpc to AU scales). The processes include the accretion of gas onto galactic disks and cooling of this gas to form a neutral phase, the formation of molecular clouds, denser clumps, and cores and the final formation of stars. Once the stars are formed, they provide feedback in form of winds, UV radiation and eventually supernova explosions, which self-regulate star formation.

Of particular observational importance are fine structure lines ([C I], [C II],]O I] and [N II]) as well as mid- and high-excitation CO lines, since they are agents of cooling in molecular cloud formation or star formation feedback, and therefore important tracers of these processes. These lines are hard to observe from the ground, since they are at submm or THz frequencies. For high-redshifted galaxies, however, they can get shifted into the ALMA bands, and are by now regularly observed as indicators of star formation activity. Yet, even with ALMA, the highly redshifted galaxies cannot be resolved beyond the kpc scale, leaving the bulk of the physical processes leading to the formation of stars in these galaxies unobservable.

To understand the star formation process in detail, even within the high-redshift galaxies, it is essential to grasp the physics of these lines in sources that can be spatially resolved, i.e. in our Galaxy and nearby galaxies.   A thorough understanding of large scale, galactic, star formation and related feedback processes is crucial to develop a self-contained theory of galaxy formation and evolution. The Galactic disk, but also in particular the Galactic Center and the Large and Small Magellanic Clouds, are important laboratories in this respect, since they allow a glimpse of star formation in normal disk molecular clouds, a galaxy core and in both normal and low metallicity environments, all of which are ingredients of star formation in the early and contemporary universe.

Star formation processes are not only subject to different spatial scales but also to a variety of environmental factors. Metallicity, temperature, pressure, dust composition, density, column density and the interstellar radiation field (ISRF) are but a few examples of parameters that vary from molecular cloud to cloud and in between galaxies. Observing different environments, in particular with different metallicities and/or different star formation activity, will be important in order to disentangle the effects. For this reason it is important to add the Magellanic Clouds as important stepping stones between observations in the Milky Way and those obtained in galaxies at higher redshifts with ALMA.
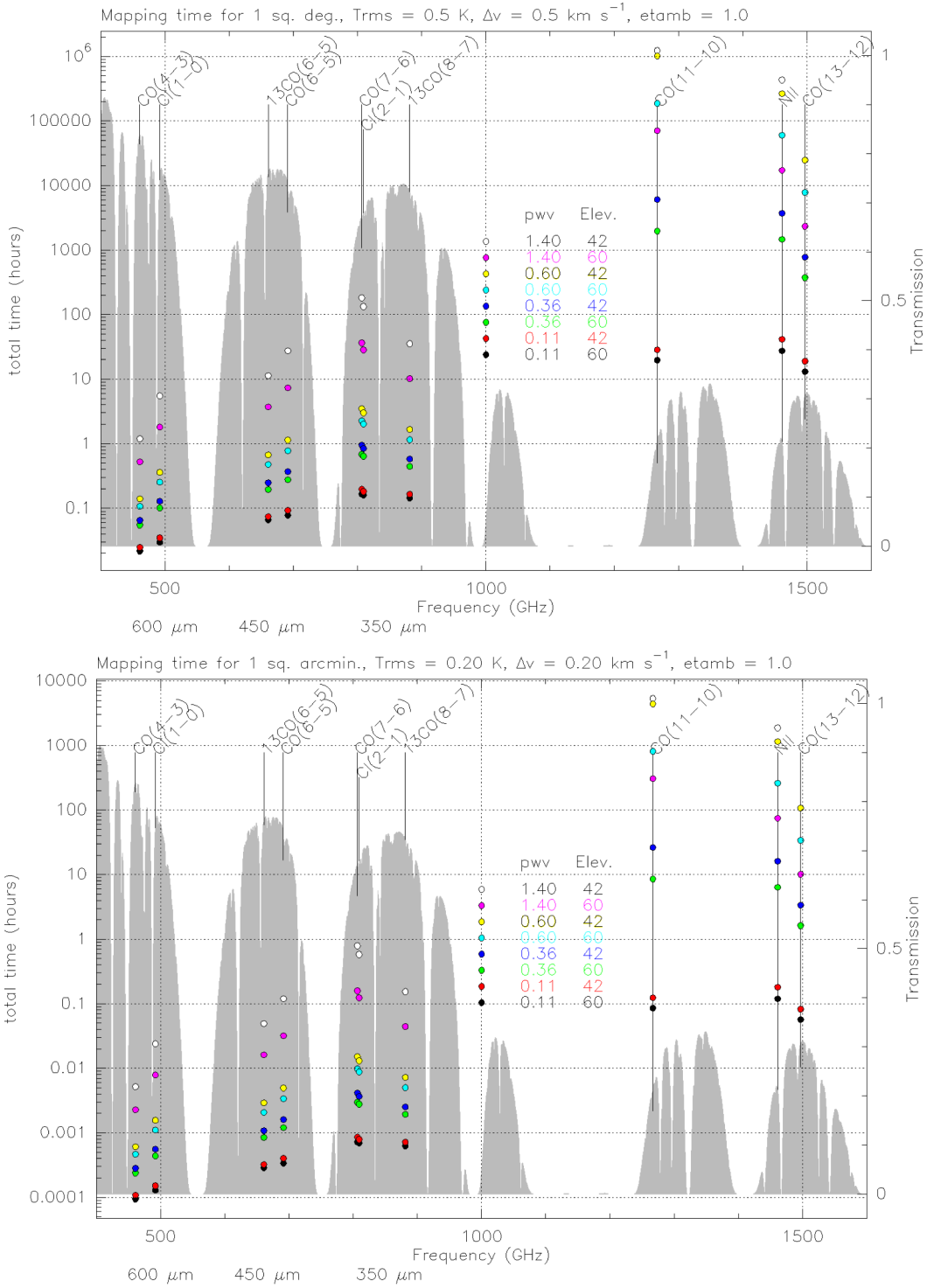
Fig. 1 Mapping times for 1 sq deg (top) to an rms of 0.5 K in a 0.5 km/s channel and for 1 sq min (bottom) to an rms of 0.2 K in a 0.2 km/s channel, for different values of the precipitable water vapor. One sees that 1 sq deg maps are within easy reach for the lines in the sub-THz windows, and maps of the CO(4-3) and [C I](1-0) line even under average or mediocre weather conditions (light blue and yellow dots, corresponding to the 75% percentile pwv of 1.4 mm at Cerro Chajnantor, which corresponds to the 50% percentile on the ALMA site), while 1 sq arcmin maps are possible at the THz windows only under good weather conditions (red and black dots), corresponding to a pwv of 0.2 mm, available 10% of the time).

In the local universe, some of these lines ([C II] and [O I]) can only be observed from the airborne observatory SOFIA, others ([C I] and mid-J CO lines[1]) can be observed from the ground (e.g. from APEX or ALMA, albeit with difficulty). [N II] and high-J CO lines can and are observed with SOFIA, but would be accessible to ground-based observatories on mountain sites with better transmission than the Chajnantor plateau (ALMA site). Such an observatory would afford more time for observations at a much lower operational cost than the airborne SOFIA. The angular resolution is also superior, provided that the telescope diameter is significantly larger than 2.5 m. With such a site, one thus would be able to observe inall high-frequency atmospheric windows. For maximum efficiency, the observatory should be equipped with large array receivers for the [C I](1-0) and mid-J CO lines, which would allow to map these transitions on degree scales, enabling complete mapping of the Galactic plane and the Magellanic Clouds. Similar arrays at higher frequencies would allow maps of the [C I](2-1), [N II] and high-J CO lines on 10' scales.

Based on the weather statistics, it can be seen that small maps (sq arcmin scale) are possible at THz frequencies for 10% of the time. Under average weather conditions, one can map lines in the 350 μm (850 GHz) window at degree scales, while the CO(4-3) lines and [C I](1-0) lines in the 600 μm window (460-490 GHz) can be mapped under almost any weather conditions at the high site. At the ALMA site, the weather conditions would permit square degree mapping only for a smaller window in time at these frequencies – the 75% percentile on the CCAT site corresponds to the 50% percentile at the ALMA site. The optimal setup would therefore be a simultaneous dual frequency array at 600 μm/350 μm for large maps under average or mediocre weather conditions, with the option of rapid switch-over to THz arrays should the weather improve to allow their use.

While the point source sensitivity of a 6 m telescope is lower than the originally envisioned 25 m CCAT telescope by a factor corresponding to the ratio of the collecting areas (i.e. 17), the situation is very different for extended, beam-filling sources. For those, the mapping speed scales as the square of the ratio of the beam size, i.e. for identical receiver arrays, a 6 m CCAT pathfinder would be able to map a given large area (not taking into account edge effects) 17 times faster than a 25 m CCAT, albeit at the price of a factor of 4 lower spatial resolution. Note, however, that a 6m-class telescope in the low-frequency THz regime (CCAT-pathfinder) has an angular resolution of about 12'', comparable to APEX or JCMT at long submm-wavelengths and to SOFIA in the mid-THz. The lower angular resolution is a price worth paying, since it enables very large areas (e.g. significant parts of the Galactic plane, the Central Molecular Zone or the entire Magellanic clouds) to be mapped in the CO(4-3) and [C I](1-0) lines, and zoom-ins in higher-frequency lines (at higher spatial resolution), and would prepare the path for deeper, higher resolution observations with a later, full-sized CCAT.

Specific science goals are detailed below.

2 The Formation of Molecular Clouds and Stars: The Role of Turbulence

2.1 Injection of Turbulence in Molecular Clouds: The Key to Cloud Formation?

How do molecular clouds form and evolve? The formation of stars, planets, and even the formation of the molecular building blocks of life itself takes place in giant molecular clouds (GMC) that contain upwards of 10^6 solar masses ($M_\odot$) of gas and dust, but the origin of these clouds themselves is still uncertain.

Long-Lived & Quasi-static GMCs: Early models suggested that GMCs are in a state of gravitational contraction. However, it was quickly realized that the predicted star formation rate in such contracting clouds is far higher than observed (Zuckerman & Evans 1974). Either GMCs are supported against collapse (e.g. via magnetic fields or turbulence) and live far longer than a dynamical time, or

---

[1] In the following, low-J CO refers to the J=1-0 to 3-2 lines, mid-J to J=4-3 to 8-7, and high-J to higher transitions.

the star formation efficiency is low, since feedback from the star formation process itself (e.g. jets, outflows, HII regions, supernova) would sustain the turbulence or disperse the cloud. The prevailing view has long been that GMCs survive for tens if not hundreds of million years (see Scoville 2012). The simplest argument in favor of long-lived clouds is continuity of mass between the various components of the Interstellar Medium (ISM): neutral atomic hydrogen (HI), ionized atomic hydrogen (HII), and molecular hydrogen (H_2). Since H_2 is the dominant mass component in the interior of the Milky Way and other galaxies, then most of the gas lifetime must be in the H_2 phase. Given that the timescale to form H_2 from HI and the time to pass between spiral arms are both on the order of 10^8 years, the inferred lifetime of the H_2 is ~10^8 yr.

Invoking long-lived clouds, however, does require a mechanism to support clouds against gravitational collapse for many dynamical lifetimes. Simulations of hydrodynamic and magnetized turbulence show that all primordial turbulent motions in a GMC are quickly dissipated on a timescale comparable to the sound crossing time (e.g., Mac Low et al. 1998; Mac Low & Klessen 2004), at which point the cloud should gravitationally collapse and form stars. Since this contradicts the observed star formation rate, the turbulent motions must somehow be sustained for long time periods via some mechanisms that constantly re-inject turbulence on timescales shorter than the sound crossing time. Magnetic fields were thought to be a stabilizing force, but recent observations suggest they are too weak to support clouds over long lifetimes (see review by Crutcher 2012). External drivers of turbulence such as HII regions and supernova have also been postulated as possible culprits. Neither of these, however, have been convincingly shown to be the main sources of turbulence in GMCs over long timescales. Turbulence also plays a role in creating the seeds of star formation, which then can collapse gravitationally.

Short-Lived & Dynamic GMCs: In part because of the difficulties in the long-lived cloud model, the notion that GMCs may be relatively short-lived structures has been re-examined (e.g., Blitz & Shu 1980; Scalo 1990; Hartmann et al. 2001). In these models, GMCs collapse on relatively short times, but the cloud is dispersed after forming relatively few stars. This dynamic scenario means that there is no equilibrium state, and the process of star formation is *intimately* linked with the process of molecular cloud formation and collapse. Support for a dynamical picture of clouds has emerged from panoramic images in both molecular lines and the dust continuum, which reveal complex structures that belie an equilibrium state (Goldsmith et al. 2008; Molinari et al. 2010). Indeed, the network of filaments that pervade the interstellar medium can be qualitatively explained by numerical simulations of magneto-hydrodynamic turbulence (e.g., Padoan & Nordlund 2011) in gravitationally infalling gas.

In their theoretical study of the growth, evolution, and dispersal of molecular clouds, Goldbaum et al. (2011) proposed that the accretion of new material from the surrounding environment can drive the observed turbulent motions in short-lived GMCs. This model is attractive since it explains why similar size-linewidth scaling relations are observed in clouds regardless of the level of star formation activity (see, e.g., Bensch et al. 2001; Heyer et al. 2006; Schneider et al. 2011; Vázquez-Semadeni 2011). This model is also consistent with observations that suggest the global filamentary structure of molecular clouds is created by large scale colliding flows of atomic material at earlier times (Wang et al. 2010; Molinari et al. 2010; Peretto et al. 2012).
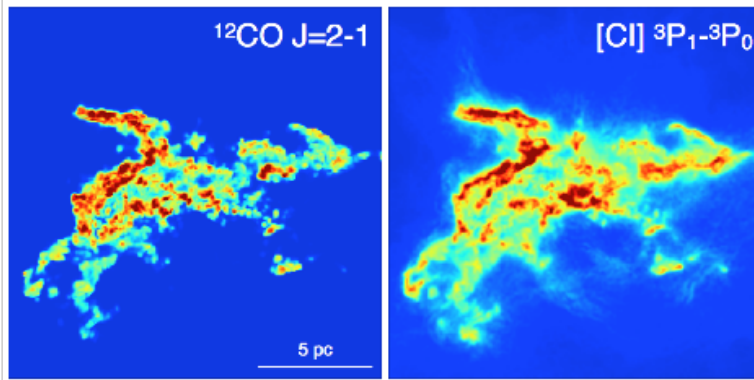
Fig. 2 Simulation of the CO J = 2-1 (left) and [CI] $^3P_1$ - $^3P_0$ (right) integrated intensity for a GMC exposed to an average interstellar ultra-violet radiation field in the inner Galaxy. In these models, the [CI] traces the cloud material in both the high density inner regions traced by CO, as well as the extended, diffuse regions that are free of CO emission but still have significant H_2 abundance. Simulations from Glover et al. 2015
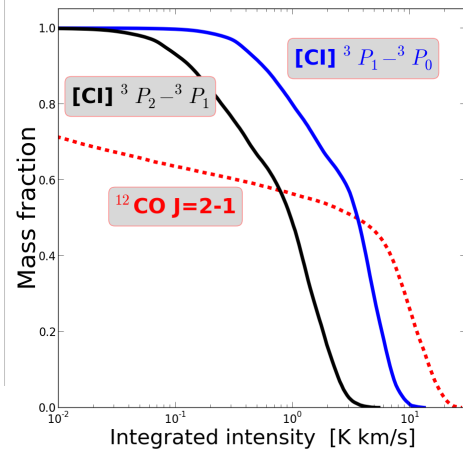

Fig. 3 The fraction of total cloud mass probed by CO and [CI] as a function of CO integrated intensity (which scales directly with density). At the edges of GMCs, where the CO integrated intensity is low (≤ 0.1 K km/s) and difficult to detect, the two ground-state, fine-structure transitions of [CI] ($^3P_2$ - $^3P_1$ at 809 GHz and $^3P_1$ - $^3P_0$ at 492 GHz) trace more than 90% of the cloud mass, whereas a commonly used transition of CO (J=2-1 at 230 GHz) only traces ~ 60-70% (Glover, priv. comm.)

Turbulence is the Key: Understanding the origin of the turbulence within GMCs is, therefore, key to understanding their formation and evolution. For typical gas temperatures of ~10K, the thermal sound speed is ~0.1 km/s yet the observed velocity dispersion is of order 1-4 km/s, a value which places in rough equipartition the gravitational binding energy and kinematic energy of the molecular cloud. The different theories for the origin and evolution of clouds are all tied to understanding the mechanisms that drive and sustain these supersonic turbulent motions. Supersonic turbulence has been attributed to a number of factors, including magnetic fields, protostellar outflows, H II regions, supernovae, and on-going mass accretion. While the first four have been examined in numerous studies, mass accretion has not been thoroughly investigated observationally.

If mass accretion is an important source of turbulence as suggested in the dynamic GMC formation scenario, this material may be accreted primarily as diffuse atomic gas. While this atomic gas can, in principle, be detected using the 21 cm atomic hydrogen line, in practice the emission is highly confused by HI in the ISM along the line of sight. A potentially valuable tracer of cloud mass accretion via atomic gas, therefore, is neutral atomic carbon [CI], which (together with ionized carbon or [CII]) should be the dominant form of this element (and the dominant atomic species other than HI) at the extinctions and densities of GMC exteriors (Pineda et al. 2010). [CI] also suffers from much less confusion due to line of sight gas not associated with the cloud being studied, than does HI.

Mass accretion onto GMCs may also occur via low density molecular hydrogen. Molecular hydrogen, however, is not detectable at the cold gas temperatures in the ISM (since it has no dipole transitions) and so carbon monoxide (CO), which is easy to measure in the ISM, is often used as a proxy for the total molecular gas content. Theoretical models predict that the formation of CO lags behind the formation of H_2. A consequence of this formation lag is the existence of "dark" or "invisible" molecular gas, containing H_2 but no CO gas. [CI] is also a tracer this "dark gas" and, therefore, of cloud mass accretion via low density molecular hydrogen as well. This is demonstrated in Figures 2 & 3, which illustrate how, in low density regimes at the surfaces or edges of GMCs, [CI] traces more of the cloud mass than CO does.

Required Observations to Address the Science Goals: Understanding the role that mass accretion may play in generating the observed turbulence in GMCs (and, hence, in their formation and evolution towards star and planet forming entities) requires high spectral resolution (< 0.1 km/s) observations of atomic and molecular emission over scales covering entire GMCs (10's to 100's of pc in size). Large scale maps of the integrated intensity emission from both carbon transitions are needed to identify clouds in the process of formation as indicated by cold regions where atomic carbon has not been fully processed into CO. Comparison of the [CI] and low energy CO maps (the latter obtained from existing surveys made, e.g., with the FCRAO or Mopra telescopes) will also assess the amount of ongoing mass accretion onto clouds in the form of both atomic and "CO dark" molecular gas. Since mass accretion is a dynamic process, these large-scale maps must also have high spectral resolution in order to measure the relatively modest velocity shifts that will trace the accretion motion onto the bulk of the molecular cloud and to fully resolve the line widths, which are expected to be in the range of 0.2 - 4 km/s. Note that observations of both [CI] transitions are required to unambiguously determine the total mass of atomic carbon. With only one transition, one would have to assume a largely unknown form for the partition function, which may result in large overestimates (or underestimates) of the true carbon and, therefore, accreting gas mass.

[CI] Excitation: The two transitions of carbon ($^3P_2$ - $^3P_1$ at 809 GHz and $^3P_1$ - $^3P_0$ at 492 GHz), have different excitation conditions. The excitation temperature and critical densities are 23.6 K and ~ 500 cm^{-3} for the 1-0 transition and 62.5 K and ~ 2500 cm^{-3} for 2-1. Therefore, the 1-0 transition should be more easily detectable in low temperature and low density environments. Observations by Plume et al. (1999) have shown that, at the edges of GMCs (defined as regions with integrated intensities < 10 K km s^{-1}), the C^o column density is < 10^{17} cm^{-2}, and line widths are ~2.5 km s^{-1}. Using these

Fig. 4 RADEX models of [CI] 1-0 (Blue) and 2-1 (Green) emission in low column density (N) and low density (n) gas for a range of kinetic temperatures.

parameters and the RADEX statistical equilibrium radiative transfer code (van der Tak et al. 2007), we have modelled the expected [CI] line intensities under a range of excitation conditions expected at the low column density edges of GMCs. The plots in Figure 4 indicate that, at very low temperatures, densities, and column densities (top left), both transitions will be difficult to detect (T_R < 0.5 K). A factor of ten increase in density **or** column density will allow the 1-0 transition to be detected fairly easily. Higher densities **and** column densities (bottom right) would be required to map the 2-1 transition. However, H$_2$ densities of ~ 10^3 cm^{-3} and C^o column densities of 10^{17} cm^{-2}, are expected throughout the bulk of GMCs (Plume et al. 1999). Therefore, while it may be difficult to map the 2-1 transition at the very edges of clouds, with the atmospheric conditions expected at CCAT-p, it will be possible to map it over moderate size-scales (~ 1 square degree) in slightly higher density/column density regions in a few hours of observing time.
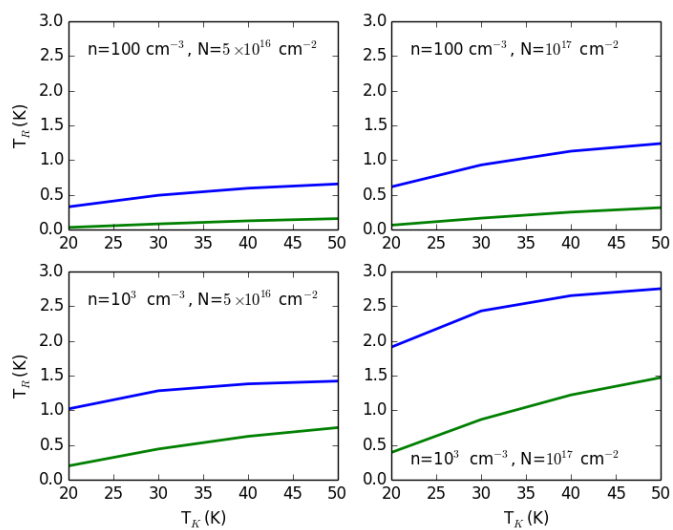
2.2   Dissipation of Turbulence in Molecular Clouds: The Key to Star Formation?

CCAT-p offers a unique opportunity to study both the dynamics and energetics of turbulent motions. Turbulence motions are ubiquitous in the interstellar medium (ISM) and carry a large fraction of the energy in the ISM. It plays the central role in establishing the structure of gas and magnetic fields in galaxies and is suggested to be the dominant regulatory factor controlling the star formation process, establishing the stellar mass function (e.g., Padoan et al., 2014). Turbulence is multi-scale by nature, transferring energy from large injection scales corresponding to the scale height of the galactic disk or the largest scales of stellar feedback ($10^{2.5}$ pc) to small scales (10^{-1} pc) where the motions become dominated by thermal motions.

Fig. 5 *Predicted CO(6-5) emission from the simulation of Offner et al. (2014) for a molecular cloud observed by CCAT-p at 250 pc. The map shows the peak brightness of the emission. The same region could be observed by CCAT-p with a noise level of 0.25 K in a 0.5 km/s channel in 1 hour (PWV=1.4 mm, elevation=60°). The CCAT-p beam is shown as a white circle. (Simulation data courtesy of S. Offner)*

A key question to be answered about turbulent flows is how kinetic energy is dissipated at different scales. Theory predicts that turbulence is highly dissipative in molecular gas, with a significant source of energy loss being line cooling in the wake of an ensemble of low-velocity shocks. To date, our large-scale surveys of molecular clouds have focused on the low-*J* spectral lines [CO(1-0), CO(2-1), CO(3-2)], where the thermal emission of the gas dominates the emission and line opacity complicates the interpretation of the results. However, the CO lines that CCAT-p can survey [CO(4-3), CO(6-5), CO(7-6)] will highlight these dissipative shocks. Targeted *Herschel* observations by Pon et al. (2014) showed anomalously bright emission from these lines that could not be explained by radiative excitation alone. Such emission can be provided by shocks, which should create ubiquitous emission at relatively low surface brightness (Figure 5).

The unique combination of CHAI on CCAT-p will provide efficient full cloud scale surveys of molecular gas in these high-*J* CO lines and reveal dissipative shocks. By measuring the radiative losses from the ensemble of post-shock gas, these surveys provide a calorimetric measurement of turbulent dissipation. CCAT-p data will provide a localized and direct measure of the energy losses from the turbulence that cannot be accessed through other means. These post shock conditions also shape the chemical histories of molecular clouds, stochastically driving gas to high densities and temperatures. Given the central role of turbulence in the ISM, finding and surveying these low-velocity shocks in molecular gas is a clear niche that can be filled by CCAT-p.

Wide area surveys of nearby molecular clouds will also untangle the different contributors to CO line emission at high-*J*. Integrated over large regions, galaxies are observed emit a significant amount of their CO luminosity in these high-*J* lines (Kamenetzky et al., 2014) with characteristic temperatures of ~10^3 K. It is unknown how much of this integrated emission arises from photon dominated regions or after coherent high-velocity shocks driven from, e.g., protostellar winds, outflows and converging flows into molecular clouds. Using wide area mapping from CCAT-p, it finally becomes possible to
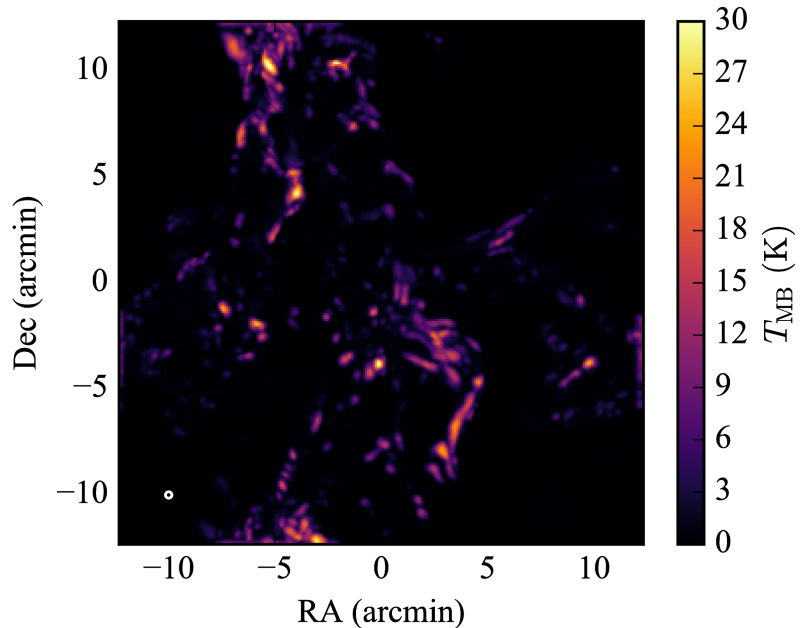
partition this emission spatially and identify the contributions to the high-*J* line emission budget. Isolating these line emission mechanisms will solidify our interpretation of high redshift CO studies which must study the high-J lines to be detected by the instruments.

While these specific lines can be observed by other telescopes, notably ALMA, it is simply prohibitive to conduct wide area surveys of this molecular emission on the relevant physical scales (0.1 to 300 pc). ALMA has too high of an angular resolution to probe this physics. CCAT-p can efficiently study local molecular clouds (<1 kpc) with degree-scale maps using the much smaller aperture of CCAT-p scaled up by the multi-receptor CHAI array. To match the same spatial dynamic range in CO(6-5), ALMA would have to study clouds at distances >40 kpc. To include all spatial scales, ALMA requires 8 times longer observing time than CCAT-p in the best ALMA weather. Instead, CCAT-p complements ALMA, enabling the identification of regions where shock processes can be examined at the small angular scales for which ALMA is designed. Thus, the turbulent energetics of the molecular ISM is a clear niche that can be filled by CCAT-p.

2.3   Observation Plan

From the discussion above, we will have two types of large heterodyne surveys. For the study of the formation of molecular clouds (Section 2.1), we will strive to map [CI] over areas that are as large as possible to have a statistically significant sample. For example, we would survey molecular clouds in the Galactic Plane covering ~200 sq deg in the [CI] 1-0 and CO(4-3) lines to a depth of 0.25 K and a velocity resolution of 0.5 km/s. We would also survey the same lines in the LMC over ~64 sq deg and SMC (20 sq deg) to a depth of 0.1 K and velocity resolution of 1 km/s (since typical measured intensities are 0.3 to 1 K; Okada et al. 2015; Requena-Torres et al. 2016). The precise surveyed areas will be determined by the extent of the sources and their visibility from Cerro Chajnantor. This would be augmented by zoom-in observations in [CI] 2-1 in areas where [CI] 1-0 is strong.

For the study of turbulence dissipation in molecular clouds (Section 2.2), the survey would target nearby clouds so that beam dilution of the shocks is minimized. Thus, Gould Belt objects would be logical targets. The survey should span an array of environments with wide area mapping. Ideally, Orion A and B would be the high mass end and Lupus presumably would be the main low mass target. However, Serpens and Ophiuchus would be good additional targets. Spanning ~ 30 square degrees would cover most of the interesting regions. To velocity resolve shocked emission we would require 0.25 km/s resolution (close to the sound speed). Since the science analysis will rely on the CO Spectral Line Energy Distribution (SLED), we intend to map as many CO lines as possible including, but not limited to: CO(4-3), CO(6-5), ^{13}CO(6-5) and ^{13}CO(8-7) over the whole survey area. We will follow up on the brightest regions with the highest J lines: CO (11-10) and CO (13-12). A 0.25 K sensitivity should detect shock emission given model output in the shock regions.

The surveys are summarized in the following table.

Survey	Line	Size	rms	Delta v	Beam	Percentile	Time (h)	Days (8 h)
Galactic Plane	CI(1-0)	200 sq deg	0.25 K	0.5 km/s	26″	50	250	31
	CO(4-3)	200 sq deg	0.25 K	0.5 km/s	26″	50	100	13
LMC	CI(1-0)	64 sq deg	0.1 K	1 km/s	26″	50	250	31
	CO(4-3)	64 sq deg	0.1 K	1 km/s	26″	50	100	13
SMC	CI(1-0)	20 sq deg	0.1 K	1 km/s	26″	50	80	10
	CO(4-3)	20 sq deg	0.1 K	1 km/s	26″	50	30	4
Gould Belt	CO(6-5)	30 sq deg	0.25 K	0.25 km/s	19″	50	240	30
	^{13}CO(6-5)	30 sq deg	0.25 K	0.25 km/s	19″	50	135	17
	^{13}CO(8-7)	30 sq deg	0.25 K	0.25 km/s	14″	25	120	15
Total							**1305**	**163**
Zoom-Ins	CI(2-1)	50 sq deg	0.25 K	0.5 km/s	16″	25	150	19
	CO(11-10)	1 sq deg	0.25 K	0.25 km/s	10″	10	96	12
	CO(13-12)	1 sq deg	0.25 K	0.25 km/s	8″	10	63	8

3 Protostellar Variability

The accepted paradigm for the birth of low-mass stars has them forming via the gravitational collapse of molecular cloud cores. The accretion rate within the core is set through an initial balance between gravity and thermal pressure, leading to a fiducial infall rate $dM/dt \propto c_s^3/G$ (Shu 1977; Shu et al. 1987). The evolution of the mass accretion onto a forming protostar, however, depends not only on the rate at which the interior of the core collapses, but also the significance of a circumstellar disk as a temporary mass reservoir, and the physics of how the gas is transported through the disk and accretes onto the central star.

One outcome of the Spitzer c2d programme (Dunham et al. 2010, 2012, 2015) was a census of nearby star-forming regions, allowing for a rough determination of protostellar lifetimes and therefore the mean accretion rate onto a typical low-mass star. Reassuringly, this derived accretion rate is similar to the theoretical value for core-collapse discussed above. The typical luminosity of observed protostars, however, has been known for two decades to fall below that required for steady accretion (Kenyon et al. 1990) and the c2d observations extend this disagreement to a much larger sample.

A number of solutions to the 'luminosity problem' have been proposed, all of which require a non-constant accretion rate onto the protostar (e.g. Vorobyov & Basu 2005, 2015; Zhu et al. 2010; Bae et al. 2014; Simon et al. 2011). As well, known protostellar variables, such as FU Ori sources, suggest that accretion may take place episodically, with material piling up in the outer disk for long periods until the disk itself becomes gravitationally unstable and the mass violently accretes in a giant burst (e.g. Hartmann & Kenyon 1996; Audard et al. 2014).

Despite a clear requirement for some form of time dependency in the accretion rate onto deeply embedded protostars and a large number of theoretical mechanisms for powering variability, our understanding of both the timescale and amplitude of variability is almost entirely unconstrained. Given that the bolometric luminosity of deeply embedded protostars is a direct proxy for the accretion luminosity, modified only by the addition of the stellar luminosity itself, monitoring the protostellar flux near the peak of the protostellar SED at ~100 microns should uncover this variability (Johnstone et al. 2013). Determination of the strength of the variability on ~year timescales would provide a direct measure of the physical processes within the disk at ~AU scales, yielding important clues to the evolution of the protoplanetary disk.

With CCAT-p it should be possible to monitor ~20 fields on month timescales for at least five years with each epoch requiring half an hour per field (~10hrs total per epoch). As the survey advances in time, each of these fields will approach a depth usually only reached in cosmological surveys. Time should also be held in reserve for target of opportunity observations of erupting young stars found through near infrared and optical surveys, with the idea being to follow these sources at day to week cadences while they remain variable.

3.1 Observation Plan

CCAT-P is being designed to operate as a continuum survey instrument between 350 and 3000 μm, with a large instantaneous field of view and an excellent sensitivity. For the variability survey we wish to observe star-forming fields using the shortest CCAT-P wavelengths (350 and 450 μm) in order to probe close to the peak of the protostellar SED. Forming stars tend to be gregarious and thus we will take individual snapshots utilizing CCAT-P's one-third of a square degree instantaneous field of view. Since we require multiple epochs, spaced roughly evenly in time, we assume that the typical observation will be performed in 2nd quartile weather. Protostars are bright at these wavelengths (typically greater than a Jansky), even at the distance of Orion, and thus we set a sensitivity requirement of 10 mJy per beam (1 sigma providing a S/N of at least 100) in each individual epoch. According to the sensitivity table provided by the CCAT-P team for the P-Cam instrument, each snapshot will require 0.85 hrs (350 microns) and 0.52 hrs (450 μm) or about 2 hrs in total, including overheads. **Three nights a month (36 nights a year)** will therefore allow **18 fields (covering 6 Square degrees in total)** to be observed on a monthly basis. Typically these fields will contain **5 to 10 deeply**

embedded protostars and 10 to 100 Class I sources. Furthermore, assuming a **five year programme**, as many as 60 epochs for each field will be observed providing afinal stacked-map sensitivity ~7 times deeper than the individual epochs.

This proposal represents a significant increase over the on-going JCMT SCUBA-2 Variability Study which observes 8 one-quarter square degree fields at 850 μm (and 450 μm during excellent weather) to a depth of ~10 mJy per beam. The CCAT-P survey will therefore image 3 times the JCMT survey area. Furthermore, given that protostars are significantly brighter at shorter wavelengths, the CCAT-P survey sensitivity limit should correspond to better than a 10-fold increase in survey depth per epoch. The greatest benefit of the CCAT-P survey, however, will be the significant advantage obtained by observing closer to the peak of the protostellar SED, where the effect of variability will be both stronger and quicker (see Johnstone et al. 2013).

4 Scientific niche: compact THz sources

Tipping meter statistics over more than a decade show that the atmospheric transmission of the Chajnantor site is good enough that for a 10% of the time the 1.3 and 1.5 THz atmospheric windows allow ground-based observations. These windows are also accessible to SOFIA which, being an airplane, has a much better atmospheric transmission resulting in much better system temperatures. However, the beam of SOFIA is larger by a factor of 6/2.5 = 2.4, and the beam filling factor for point sources $(6/2.5)^2$ = 5.8 times smaller. So, CCAT-p would have an advantage if a resolution improvement of 2.4 is achieved. This is relevant for resolving small structures, e.g. high-J CO in outflows or PDRs. If the system temperature of SOFIA is less than a factor of 5.8 better than for CCAT-p, also the point source sensitivity is better. In the following tables we calculate when this is the case:

Tsys(DSB) in K						Point source equivalent SOFIA Tsys	CCAT time/SOFIA time		
Freq. (GHz)/line	Elevation	CCAT-p, pwv (mm)			SOFIA, pwv (mm)		0.2 mm	0.4 mm	0.7 mm
		0.11	0.36	0.6	0.014				
1035	50	3000	18000	95000	2500	14400	0.043	1.563	43.52
1350	50	2800	14000	62000	2400	13824	0.041	1.026	20.11
1500	50	3000	15000	70000	2500	14400	0.043	1.085	23.63
NII	50	4400	32000	100000	2600	14976	0.086	4.566	44.59
Trec (DSB) / K		500			1100				

Therefore, if the pwv < 0.4 mm (which is the case more than 25% of the time), CCAT-p is better, sometimes even significantly better, than SOFIA for point sources. This is relevant e.g. for absorption toward strong continuum sources (relevant for detections of e.g. H_2D^+), but also for detections of very compact emission of highly excited lines. This usage will not constitute a major fraction of CCAT-p observing time, but is a very attractive and important niche. This would complement SOFIA science, mostly because the CCAT-p accessible frequency range is more limited, but would also

create a fallback solution – at least for the accessible frequencies – for the unfortunately not completely unthinkable case that SOFIA does not survive the major review in 2018.

References:

Bensch, F., J. Stutzki, & V. Ossenkopf 2001, *A&Ap* 366, 636–650.

Blitz, L., & F. H. Shu 1980, *ApJ* 238, 148–157.

Crutcher, R. M. 2012, *ARA&A* 50, 29–63.

Dunham et al. 2015 ApJS, 220, 11

Dunham et al. 2012 ApJ, 747, 52

Dunham et al. 2010 ApH, 721, 995

Glover et al, MNRAS 2015, 448, 1607

Goldbaum, N. J., M. R. Krumholz, C. D. Matzner, & C. F. McKee 2011, *ApJ* 738, 101.

Goldsmith, P. F., M. Heyer, G. Narayanan, R. Snell, D. Li, & C. Brunt 2008, *ApJ* 680, 428

Hartmann & Kenyon 1985, ApJ, 299, 462

Hartmann, L., J. Ballesteros-Paredes, & E. A. Bergin 2001, *ApJ* 562, 852–868.

Heyer, M. H., J. P. Williams, & C. M. Brunt 2006, *ApJ* 643, 956– 964.

Johnstone et al. 2013, ApJ, 765, 133

Kamenetzky et al., ApJ, 795, 174

Mac Low, M.-M., & R. S. Klessen 2004, *Reviews of Modern Physics* 76, 125–194.

Mac Low, M.-M., R. S. Klessen, A. Burkert, & M. D. Smith 1998, *Physical Review Letters* 80, 2754–2757.

Molinari, S., B. Swinyard, J. Bally, et al 2010, *A&Ap* 518, L100.

Offner et al., MNRAS, 440, 81

Okada et al. 2015, A&A 580

Padoan,P.,& A Nordlund 2011, *ApJ,* 730, 40.

Peretto, N., P. André́, V. Ko̎nyves, N. Schneider, D. Arzoumanian, P. Palmeirim, P. Didelon, M. Attard, J. P. Bernard, J. Di Francesco, D. Elia, M. Hennemann, T. Hill, J. Kirk, A. Men'shchikov, F. Motte, Q. Nguyen Luong, H. Roussel, T. Sousbie, L. Testi, D. Ward-Thompson, G. J. White, & A. Zavagno 2012, *A&Ap* 541, A63.

Pineda, J. L., P. F. Goldsmith, N. Chapman, R. L. Snell, D. Li, L. Cambre̍sy, & C. Brunt 2010, *ApJ* 721, 686–708.

Plume, R., Jaffe, D. T., Tatematsi, K., Evans, N. J., & Keene, J. 1999, ApJ, 512, 768

Pon et al., 2014, MNRAS, 445, 1508

Requena-Torres et al. 2016, A&A 589

Scalo, J. 1990, In R. Capuzzo-Dolcetta, C. Chiosi, & A. di Fazio (Eds.), *Physical Processes in Fragmentation and Star Formation*, Volume 162 of *Astrophysics and Space Science Library*, pp. 151–176.

Schneider, N., S. Bontemps, R. Simon, V. Ossenkopf, C. Federrath, R. S. Klessen, F. Motte, P. André́, J.

Stutzki, & C. Brunt 2011,*A&Ap* 529, A1.

Scoville, N. Z. 2012. *ArXiv e-prints*.

Va´zquez-Semadeni, E. 2011, In J. Alves, B. G. Elmegreen, J. M. Girart, & V. Trimble (Eds.), *Computational Star Formation*, Volume 270 of *IAU Symposium*, pp. 275–282.

Van der Tak, F.F.S., Black, J.H., Schöier, F.L., Jansen, D.J., van Dishoeck, E.F. 2007, A&A 468, 627

Vorobyov & Basu 2010, ApJ, 719, 1896

Wang, P., Z.-Y. Li, T. Abel, & F. Nakamura 2010, *ApJ* 709, 27–41.

Zuckerman, B., & N. J. Evans, II 1974 *ApJ* 192, L149–L152.